STM JOURNALS

Trends in
Machine Design

ISSN: 2455-3352
Volume 12, Issue 3, 2025
September–December
DOI (Journal): 10.37591/TMD

https://journals.stmjournals.com/tmd

Research TMD

# Analysis of Die Corner Gap Formation for Strain Hardening Materials in ECAP Through an Upper Bound Sensitivity Approach: A Comparative Study

Nagendra Singh[1], Manoj Kumar Agrawal[2], Manish Dixit[3,*], Saurabh Pachauri[3]

**Abstract**

*In recent work, using a proposed $2^k$ central composite factorial analysis, the upper-bound theorem's theoretical concept for the equal channel angular pressing process are used. The upper-bound theorem-based theoretical solutions consider Tresca friction conditions and varied fillet radii at the die channel junction. When using AA5083's uniaxial mechanical properties, isotropic nonlinear work hardening is assumed. The ratio of the cumulative effective plastic strain to the time generated by the deformation zones, the effects of strain rate are considered in equal channel angular pressing. In equal channel angular pressing, the load is estimated using an isotropic yield criterion. The billet experiences a simple shear stress state in the equal channel angular pressing process; a noticeable impact of the tooling frictional conditions is evident. Higher values of the ratio between the yield stresses in uniaxial tension or compression and pure shear, or extreme friction conditions, lead to higher levels of equal channel angular pressing load. The suggested composite $2^k$ factorial analysis enables the examination of the primary parameters influencing both the pressure and load in equal channel angular pressing. The outer and inner fillet radii, primarily govern the effective plastic strain. Consistent theoretical predictions indicate that incorporating work-hardening behavior into models, regardless of tribology or tooling arrangements, results in decreased forecasts for pressing force and effective plastic stresses as well as greater die corner $\psi$ angle values. At the deformation zone entrance surface, the immediate workpiece height is related to both the pressing force and the effective plastic strain.*

**Keywords:** Upper bound analysis, factorial analysis, plasticity criterion, ECAP, die corner angle

## INTRODUCTION

ECAP is a severe plastic deformation process used to create bulk materials with ultra-fine grain structure and better mechanical properties. The ECAP procedure involves forcing a suitably lubricated billet through a two-channel die with a constant cross-sectional area. In the deformation zone where the die channels meet, the workpiece is subjected to a significant amount of plastic strain due to simple shear. Therefore, comprehending the fundamental ideas guiding grain refinement in the ECAP process requires a grasp of the kinematics of deformation. The literature presents models that attempt to explain the mechanics and patterns of deformity resulting from the ECAP process. Initially, macroscopic deformation models, utilizing classical analytical solutions in metal forming, such as the upper bound theorem and the slip-line field, employed the slip-line field theory for the analysis of deformation modes. Considering friction behavior, diverse tooling designs, and back-pressure in single and multi-pass ECAP processing

***Author for Correspondence**
Manish Dixit
E-mail: manishdixit90@gmail.com

[1]Assistant Professor, Department of Mechanical Engineering, Ganeshi Lal Aggarwal University, Mathura, Uttar Pradesh, India
[2]Research Scholar, Department of Mechanical Engineering, Ganeshi Lal Aggarwal University, Mathura, Uttar Pradesh, India
[3]Research Scholar, Department of Mechanical Engineering, Institute of Engineering and Technology, Khandari Campus, Agra, Uttar Pradesh, India

Received Date: September 20, 2025
Accepted Date: October 04, 2025
Published Date: November 03, 2025

**Citation:** Nagendra Singh, Manoj Kumar Agrawal, Manish Dixit, Saurabh Pachauri. Analysis of Die Corner Gap Formation for Strain Hardening Materials in ECAP Through an Upper Bound Sensitivity Approach: A Comparative Study. Trends in Machine Design. 2025; 12(3): 1–22p.

routes, the loading history is examined for a perfectly plastic material. The evolution of shear planes in successive passes or the distribution of strain are both strongly influenced by the type of processing route. This results in the formation of small shear bands with high-angle borders, which are crucial for regulating the micro-scale structural grain refinement. It was confirmed that contact friction has a major impact on strain uniformity in the specific instance of a die design with a sharp corner. Furthermore, maximizing friction can lead to a simple shear deformation mode in the flow direction. Assuming no friction and incorporating an outer die corner radius, the accurate prediction of ECAP pressure requires consideration of the material's nonlinear work-hardening behavior. Their analytical solution, grounded in the upper-bound theorem, corresponds favorably with numerical forecasts obtained from a finite element model of plane strain. In order to assess the effects of equal fillet die radii placed at the die channel intersection, the model uses finite element simulations using the upper bound theorem. Up to a maximum value, the effects of the material's work hardening and the benefits of adding a non-zero inner die corner radius were demonstrated. When this threshold is crossed, bending becomes the main deformation mode. First, the upper-bound theory was used to evaluate the impact of producing a dead metal zone in an outer sharp corner die. The study explored how friction conditions and the die's inner corner radius influence the formation of the ECAP deformation zone and the resulting strain inhomogeneity by varying the friction factor and assuming a fully plastic material. Four different slip-line field models are used to evaluate the shear strain in the deformation zone, taking into consideration both round and sharp corner dies. In reference to the former, a robust association was seen between the measured shear strains obtained from AA5083 billets that were scribed. An analytical and numerical investigation was carried out on a novel die geometry, termed "inverted ECAP," in which the outer corner radius is smaller than the inner radius. The effective von Mises strain per pass increased by over 11% when the inner and outer radii were set at 4.0 and 1.5 mm, respectively. The first upper-bound solution took into account nonlinear work-hardening behavior as well as friction circumstances for a die geometry that contained only the outer die corner radius. For a given friction factor, it was discovered that as the outer die corner radius grows, so do the normalized pressing pressure and effective von Mises plastic strain. This is due to changes in the die channels angle which varies from 90 and 135°. The intersection angle of the die channels has a greater effect than other geometrical parameters and frictional circumstances [1].

The experimental data obtained for die configurations with both round and pointed corners (AA5083) was in good accord with their upper-bound model. The study examined the formation of dead metal zones in sharp-corner dies and identified a direct relationship between the strain produced in each ECAP pass and the friction factor associated with minimizing the pressing force. In comparison with earlier findings, this latest analytical upper-bound solution showed a more favorable alignment with the measured load. All conceivable die configurations are included in the theoretical formulas developed for shear strain calculations. When the inner radius is 2.67 times greater than the outer die fillet radius, the scientists showed that the effective plastic strain per pass increases by over 11%. Recently, upper-bound solutions for the pressing pressure have been developed that take into account friction effects in completely plastic materials and cover all possible die shape configurations. The pressing pressure levels and the effective plastic strain both rise with the inner fillet radius. The flow models determine the actual strain history during the ECAP process based on descriptions of deformation kinematics. In this case, polycrystalline plasticity approaches can easily evaluate the crystallographic texture and microstructural evolution associated with deformation histories from different ECAP paths. Using continuum models and the finite element method, the effects of pertinent parameters, such as the ECAP die's geometry and the friction conditions, were examined. Apart from the production conditions, the mechanical properties, temperature fluctuations, pressing force, grain refinement, and billet stress-strain distributions are also examined. There is a requirement for more comprehensive modelling techniques to elucidate the impacts of key parameters influencing the mechanical properties and strains arising from the ECAP process. The potential coupling effects between die geometry, billet material, and friction conditions, a sensitivity analysis is recommended. Considering all of the material and processing parameters involved in ECAP, the macroscopic deformation models seem to be the best option. It is possible to assess the influence of coupling effects between geometrical, frictional, and ECAP process parameters by using the central composite factorial $2^k$ design in a sensitivity analysis.

 

First, generic solutions for the ECAP process are established by applying the upper bound theorem to the analytical modelling. A well-lubricated billet, frequently with a square cross-section, is used in the process. It is designed to pass through a two-channel die with an intersection angle ($\psi$) using a ram plunger [2, 3]. As a function of the die corner angle of curvature, the imposed shear strain on the workpiece in a single pass for an oblique intersection in the ECAP die with an angle is calculated. ($\Psi$) is located between ($\psi$)=0 and ($\psi$)=$\pi$–$\phi$, as seen in Figure 1. The following is the definition of the corresponding von Mises equivalent plastic strain:

$$\bar{\varepsilon} = \frac{1}{\sqrt{3}}\left[2\cot\left(\frac{\phi+\psi}{2}\right) + \psi\operatorname{cosec}\left(\frac{\phi+\psi}{2}\right)\right] \quad (1)$$

When working with ECAP die designs that feature an outside corner radius, the angle in Eq. (1) must be used as the workpiece's arc of curvature rather than the die corner angle. This adjustment is necessary because there is now a gap at the corner where they die and the workpiece meet. If this is not done, the associated strain may be overestimated until the workpiece fills the die completely, as was the case with the equal channel angular pressing technique with back-pressure. Based on plane-strain finite element simulations, it is found that when the strain-hardening rate of the material increases, a greater die corner gap appears in a single pass of the ECAP process for a die shape with sharp corners. When compared to a non-hardening material, this adverse effect results from a more unequal distribution of strain across the workpiece's inner and outer portions. Thus, it reduces the average equivalent plastic strain generated. For a non-hardening billet material, the conditions for the creation of the deformation zone in ECAP with an intersection die angle $\phi$=90° are investigated, taking into consideration the inner die radius and the friction between the workpiece and die walls in the channels. The variable $\psi$=$\pi$–$\phi$ characterizes the extent of the deformation zone [4].

$$\psi = \left[\frac{\pi}{2} - 2\phi\right] = \frac{\pi}{2} - 2\,tan^{-1}\sqrt{\frac{(1-m)+(1+m)(\zeta/a)}{(1+m)}} \quad (2)$$

If the angle ($\phi$) denotes the deformation zone, *(m)* stands for the friction factor, and ($\zeta$) for the inner die corner radius's origin. Strong friction between the workpiece surfaces and the ECAP die walls causes a wider deformation zone between the two die channels, as Eq. (2) predicts.

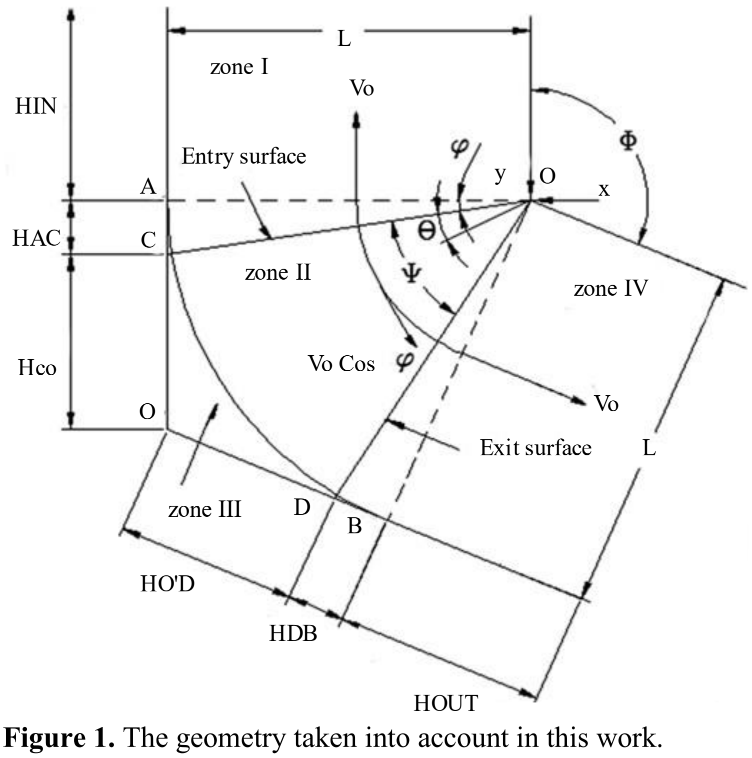


**Figure 1.** The geometry taken into account in this work.

 

As seen in Figure 1, where the die has sharp corners ($\zeta/a$=0), the entire deformation of the billet material takes place in three separate phases. The variable $m \geqslant (\zeta/a)/(2-\zeta/a)$ is necessary for the deformation zone to form. The creation of the dead metal zone in sharp corners of die the ECAP technique is analyzed, taking into account friction conditions, material strain hardening, and angle of corner *($\phi$)*. This study applies the von Mises criterion along with the average shear flow stress obtained from the Hollomon law. The angle of the deformation zone is evaluated and expressed as a function of the channel angle (ϕ) and the friction factor (m) as follows.

$$(\psi) = 2\,cotan^{-1}\left(\frac{(1-m)}{(1+m)} - (\psi)\right)^{1/2} \tag{3}$$

where the value of $m \geq \left[\frac{1-\text{cotan}^2(\phi/2)}{1+\text{cotan}^2(\phi/2)}\right]$ is the crucial condition for the creation of the dead metal zone in a die with sharp corners, and $90° \leqslant (\phi+\psi) \leqslant 180°$ is controlled by the friction factor $0 \leqslant m \leqslant 1$.

In a single pass of an ECAP die shape with ϕ=90° and inner corner radius, the effects of the strain hardening exponent (n) and the strength coefficient (MPa) in Hollomon's rule on the creation of the corner gap and the ensuing strain uniformity are investigated [5–7].

Following multivariate regression analysis and finite element predictions, the following analytical formula is obtained for the die corner angle (Figure 2):

$$\alpha = 0.02K + 75.43n + 0.09Kn(1-n) + 15.43° \tag{4}$$

When the die corner angle of curvature (ψ) is equal to the die angle predicted by Eq. (4), advantages include a more uniform strain distribution and a lower ram pressure. Taking into account the theoretical and numerical solutions offered for the die corner angle of curvature X, which establishes the dimensions of the deformation zone and has a major impact on the billet material's following strain uniformity. Therefore, it is a crucial parameter to optimize the design of ECAP dies, and work-hardening material solutions are currently not comprehensive (Figure 3).

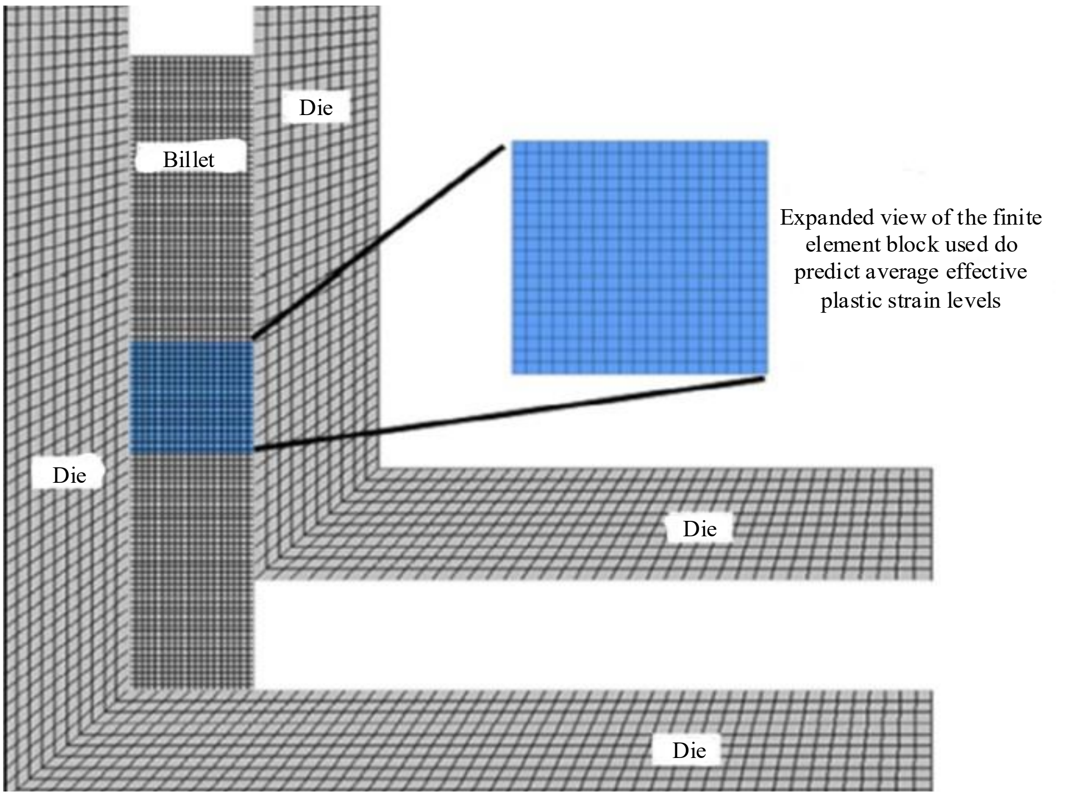


**Figure 2.** The current work proposes a finite-element model.

 

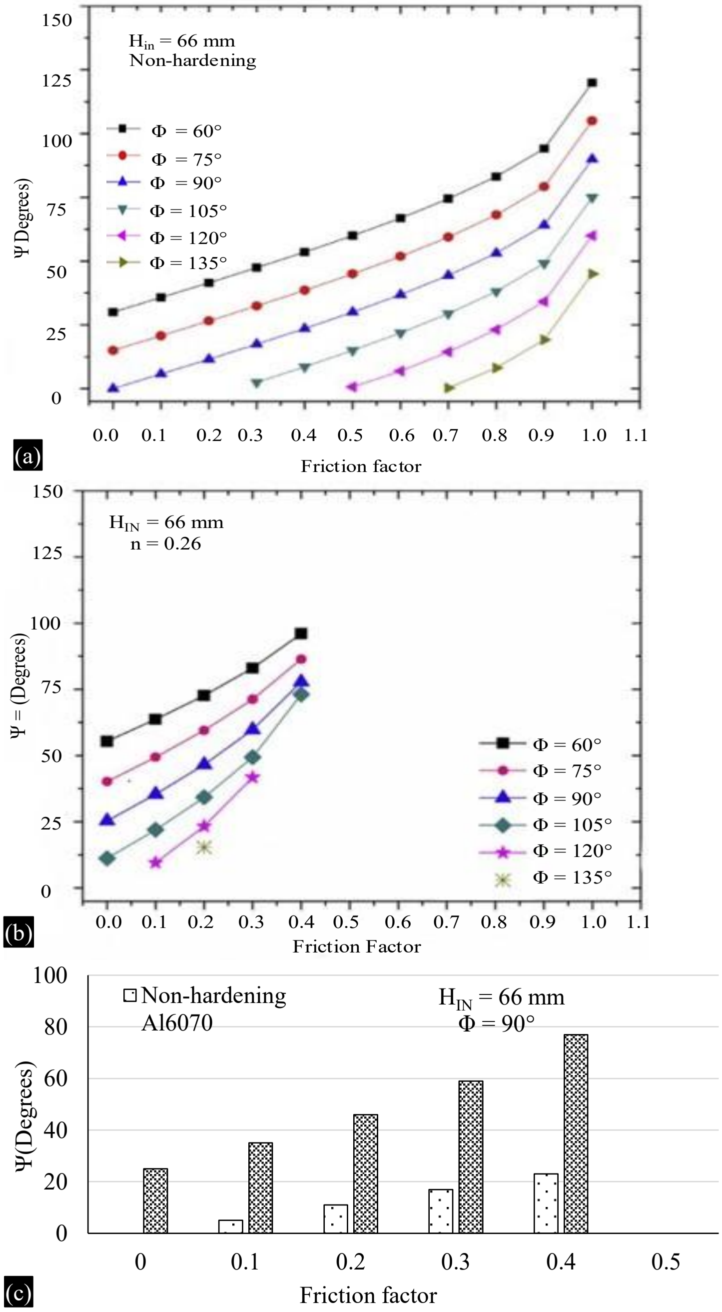


**Figure 3.** In (a) non-hardening AA5083, (b) hardening AA5083, and (c) a comparison between non-hardening and hardening alloys for (ϕ)=90° and m=0.18, analytical predictions for the die channel angle (ϕ) and the angle associated (ψ) with tribology are shown.

## ECAP Analytical Modelling

### *Pressing Pressure*

The calculations for pressing pressure (p), considering all potential die designs and incorporating frictional effects, are revisited. The die geometries analyzed are illustrated in Figure 4, where the line O serves as the local origin for both the ($R_{inner}$) and outer ($R_{outer}$) fillet radii. (B) represents the angle at where the die channels intersect, as well as the (β) angle associated with fillet radii values that are not zero. The radial and horizontal directions are defined by the parameters (r) and (x). Assuming constant velocity $V_0$ for the plunger and material point q, theoretical projections for the pressing pressure of rectangular samples are produced, accounting for the material point q and its position vector O'q.

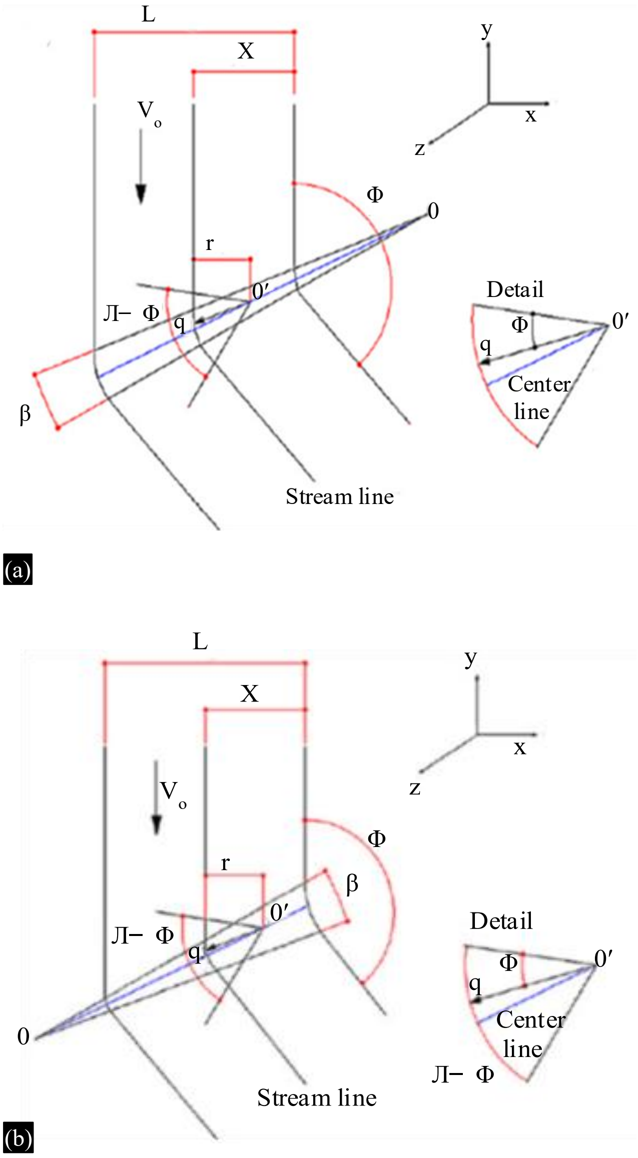


**Figure 4.** Die geometries considered in the solutions for pressing pressure: (a) $R_{inner}<R_{outer}$ and (b) $R_{inner}>R_{outer}$.

***Material Behavior***

The isotropic, temperature-independent behavior of the billet material is expected to involve nonlinear work-hardening with strain-rate effects. Thus, the yield function and the plastic loading condition determine the ECAP pressure (P). The geometry of the yield surface is given by a first-degree homogeneous function of the Cauchy stress tensor, which is defined as y, the uniaxial yield stress as a function of equivalent plastic strain and strain-rate scalar measurements. The von Mises yield criterion, based on the second invariant of the deviatoric stress components of the Cauchy stress tensor, provides a criterion for in-plane pure shear. The isotropic yield criterion is derived from the combination of the second and third invariants of the Cauchy stress tensor deviatoric stress components for the yield locus convexity [8–11]. A positive c-value permits flattening at pure shear and plane-strain tension/compression stress states, as well as rounder yield locus geometries in the vicinity of equi-biaxial tension/compression. The yield criteria can adequately characterize the crystallographic yield loci of both isotropic FCC and BCC metals. It is expected that the parameter c has a value of 2.0. This value has been adjusted to match the found isotropic FCC yield locus (Figure 5).

 

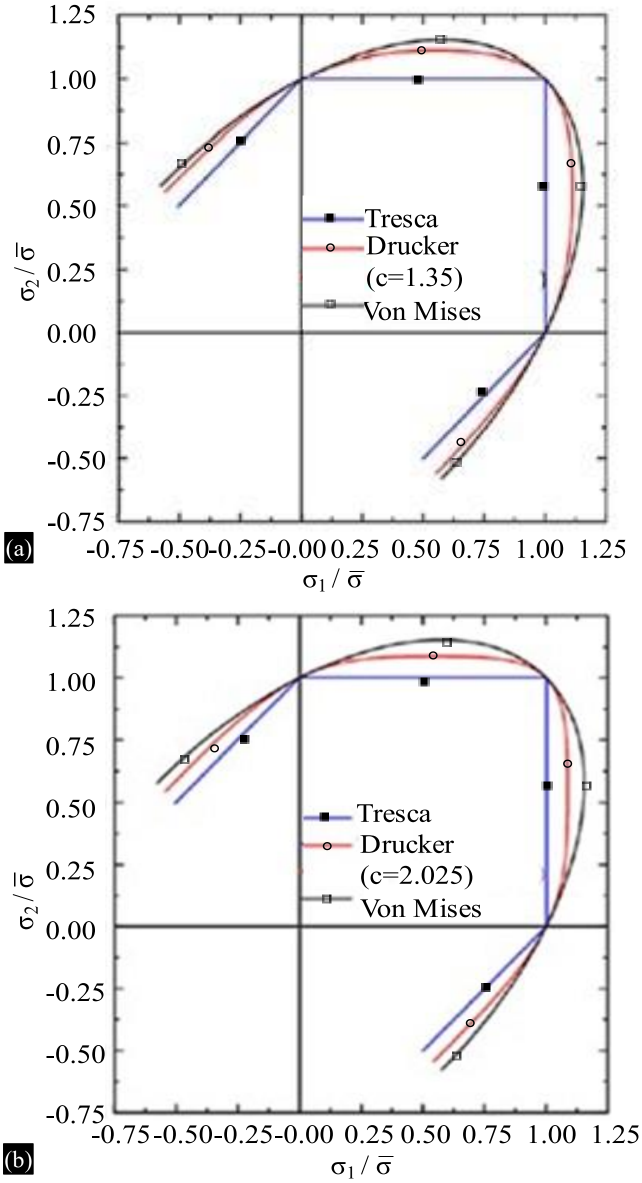


**Figure 5.** Yield surfaces in the plane-stress space for (a) BCC and (b) FCC metals are shown, normalized by the equivalent stress determined by isotropic yield criteria.

The uniaxial tension yield stress $\sigma_y$ and the in-plane pure shear yield stress, which are determined using Drucker's yield criterion, are calculated using the average stress obtained from the material's Swift hardening law. By adding the residence time in the ECAP deformation zone, the effective plastic strain takes the strain-rate impact into account. This law incorporates multiplicative strain-rate sensitivity. The strain-rate sensitivity exponent and the work-hardening exponent are numerically solved using the trapezoidal approach in order to increase forecast accuracy. On the basis of a total time derived from the geometry of the ECAP deformation zone, this assumption is then accepted. Since the plastic strains created by the ECAP process are so much more than the elastic strains, the latter can be ignored [12].

***Effective Plastic Strain***

Assuming isotropic work-hardening, the relevant flow rule is applied to the yield function to determine the plastic strain-rate components. Realizing that the von Mises and Drucker yield requirements are both stress functions of the first degree of homogeneity, the plastic multiplier is taken into account. The yield function is first subjected to Euler's identity in order to get the plastic multiplier.

 

Then, using the analogous plastic work-rate idea, it is demonstrated that the plastic multiplier is equal to the effective plastic strain-rate conjugated to the effective stress measure. Interestingly, the third invariant of the deviatoric stress components of the Cauchy stress tensor and the von Mises yield requirements offer the same effective plastic strain-rate measure in a pure shear stress condition (Figure 6).

Moreover, the plastic shear strain-rate components are specified as ($V_0/x$) within the regions AEB and DFC, (x=L), assuming an in-plane pure shear stress condition with a constant shear strain rate. Likewise, the corresponding shear strain contribution for section ABCD is equal to($V_0/r$).

***Deformation Time***

The billet undergoes significant plastic deformation around the intersection of the die channels which depends on the contributions from the regions AEB, ABCD, and DFC (Figure 6). Furthermore, it is assumed that the lengths of the AE and DF input and outlet surfaces are the same. The time gap between the outflow and inlet surfaces is calculated taking into account the continuous kinematically permissible velocity field seen in Figures 4 and 6, which is characterized by a constant velocity ($V_0$). The time within the region ABCD, as indicated in Figure 6 [13].

***The $2^k$ Factorial Design of Experiments***

The time gap between the inlet and outflow surfaces is calculated taking into account the continuous kinematically permissible velocity field seen in Figures 4 and 6, which is characterized by a constant velocity ($2^k$). The goal of obtaining a regression function for the variables is under investigation. In this experimental strategy, the impact of each parameter K on the selected variable is assessed at two levels, i.e., lower and higher values. To perform a central composite design analysis, both the central and axial points need to be taken into account. All possible pairings between the parameters are determined based on the total number of parameters considered, and the simulations or experiments are repeated to obtain the variables' responses. Using multilinear models to suggest a response surface and highlighting the significant effects of the parameters under consideration, a variance analysis driven by these effects will demonstrate their significance. The parameters influencing the ECAP pressing pressure and the effective plastic strain include the die geometry ($R_{inner}$, $R_{outer}$, and $\phi$). Other factors affecting the ECAP pressing pressure and the effective plastic strain are the plunger velocity and the friction conditions, which are defined by the Tresca friction factor.

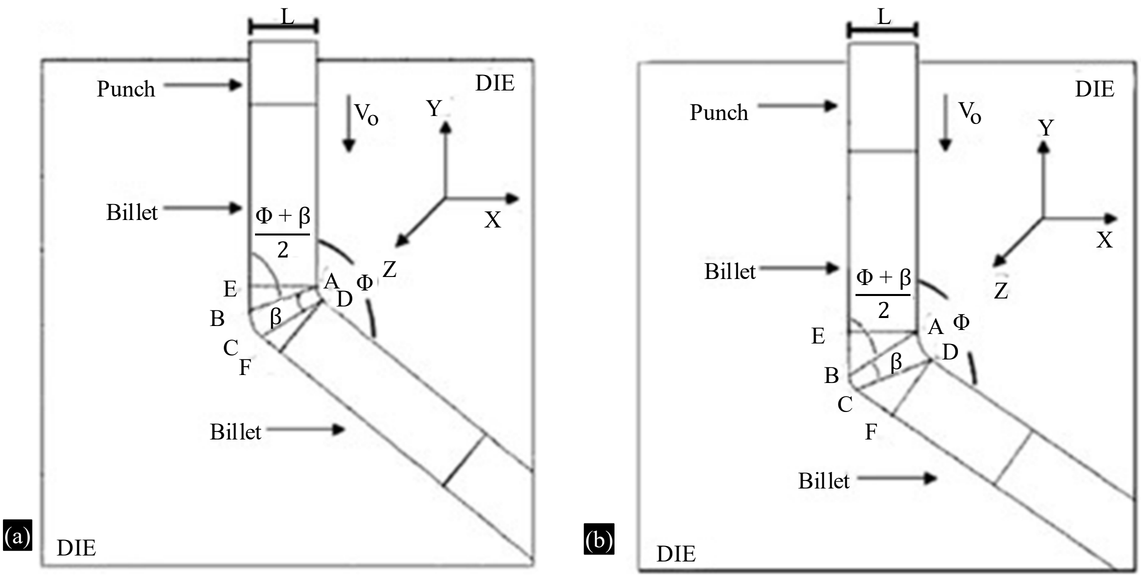


**Figure 6.** Die configurations depicting the surfaces intended for pressing time calculations: (a) $R_{inner}<R_{outer}$ and (b) $R_{inner}>R_{outer}$.

 

The corresponding values for these parameters are provided in Table 1. The rotatability parameter must be taken into account when incorporating central and axial points into factorial analysis. To find any interactions between the primary parameters given in Table 1, a curvature analysis is conducted. The factorial design is categorized as quantitative when these interactions are present because of the increased discrepancy between the average of the factors and the average of the central points [14–16].

***Theoretical Analysis***

The extension of upper-bound models is part of the theoretical analysis carried out in this work. Nonlinear work-hardening must be included in order to forecast processing load, die corner angle, and effective plastic strain under different friction conditions. The suggested approach for determining the pressing force F is provided as follows:

$$F = \frac{L^2\psi}{\sqrt{3}}\overline{\sigma_{DZ}} + \frac{L^2\sigma_y}{\sqrt{3}}cotan\left[\frac{\phi+\psi}{2}\right] + \frac{L^2}{\sqrt{3}}\overline{\sigma_F}cotan\left[\frac{\phi+\psi}{2}\right] + \frac{L^2\psi}{\sqrt{3}}\overline{\sigma_{DZ}} + \frac{L^2 m}{\sqrt{3}}\sigma_y cotan\left[\frac{\phi+\psi}{2}\right] + \frac{L^2 m}{\sqrt{3}}\overline{\sigma_F}cotan\left[\frac{\phi+\psi}{2}\right] + \frac{4mLH_{IN}}{\sqrt{3}}\sigma_y + \frac{4mLH_{OUT}}{\sqrt{3}}\sigma_y \quad (6)$$

Where L, $\mathrm{H_{IN}}$ and $\mathrm{H_{OUT}}$ represent Figure 1 for the die channel width and the surface instantaneous billet height at the entry and exit deformation zone surfaces, respectively. A value of 14 mm was assumed for (L). Furthermore, ($\sigma_y$) denotes the yield stress of the material as received; for AA5083, it was measured to be 70 MPa (Figure 7).

In addition, there is the die channel intersection angle and the friction factor. Additionally, the volumetric incompressibility indicates the friction factor and the junction angle of the ($\phi$) is the die channels, allowing the instantaneous heights $H_{IN}$ and $H_{OUT}$ to be related. The following relationship between the instantaneous heights $H_{IN}$ and $H_{OUT}$ is made possible by the volumetric incompressibility:

$$\mathrm{H_{OUT}} = \mathrm{H_{INITIAL}} - \mathrm{Lcotan}\left[\frac{\phi}{2}\right] - \mathrm{H_{IN}} \quad (7)$$

where Hout represents the total height of the billet, assumed to be 80 mm, and $H_{IN}$ was taken as $H_{INITIAL}$-L=66 mm for the purpose of comparing the non-hardenable and hardenable behaviors with the specified AA5083. Similarly, for materials exhibiting constant flow stress, where ($\sigma_y$) and ($\overline{\sigma_F}$) are both equal to ($\overline{\sigma_{DZ}}$), and by introducing the parameter H=$H_{IN}$+$H_{OUT}$+L {cotan ($\phi$/2)–1}.

Eq. (6) reverts to the one proposed in the reference mentioned. Using the von Mises criterion and the effective stresses determined by Eq. (5), the effective plastic strain was calculated using the I Wahashi *et al [2].* approach, as illustrated in Eq. (1) (Figure 8). The die corner angle was calculated by minimizing Eq. (6), which can be written as follows:

$$\frac{\partial \mathrm{F}}{\partial \psi} = 0 \quad (8)$$

**Table 1.** List of the parameters utilized in the $2^k$ factorial design employed for the ECAP process.

| Parameter | Letter for the combination | Adopted levels | | | | |
|---|---|---|---|---|---|---|
| | | *Low* | *Center* | *Axial (-)* | *Axial (+)* | *High* |
| $R_{outer}$ (mm) | (a) | 4.8 | 6.8 | 0.8543 | 11.3679 | 8.8 |
| $R_{inner}$ (mm) | (b) | 4.8 | 6.8 | 0.8543 | 11.3679 | 8.8 |
| $\phi$ (degrees) | (c) | 90 | 115 | 79.8 | 150.38 | 14 |
| f | (d) | 0.10 | 0.12 | 0.024860 | 0.32625 | 0.27 |
| $V_0\left(\frac{mm}{s}\right)$ | (e) | 3.8 | 4.78 | 0.88870 | 7.8348 | 6.2 |

 

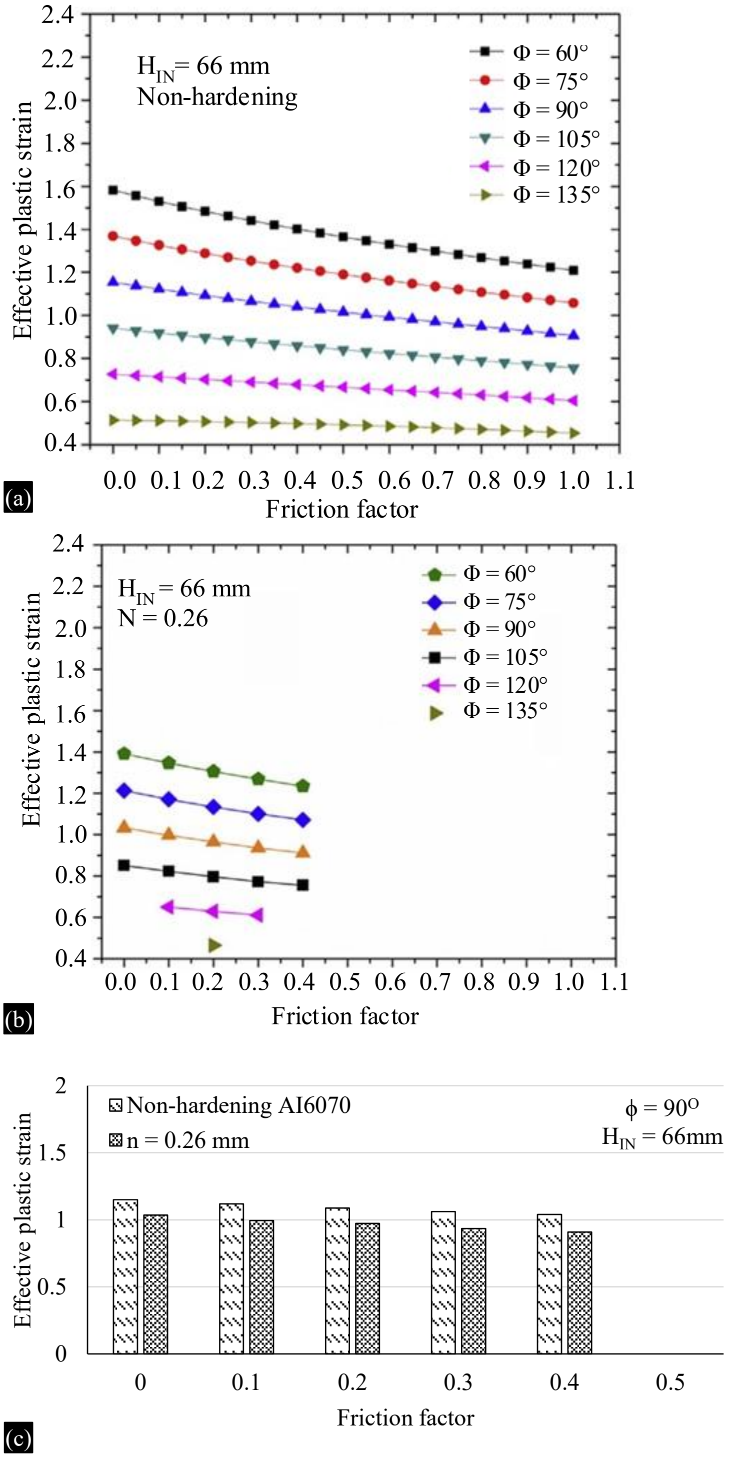


**Figure 7.** Tribology and die channel angle (ϕ) analytical estimations of effective plastic strain are presented for the alloys: (a) non-hardening AA5083, (b) hardening AA5083, and (c) a comparison between non-hardening and hardening alloys for (ϕ)=90° and m=0.18.

The angle (ψ) can be found by deriving a nonlinear expression by replacing Eq. (8) with (6).

A 90° Fortran-based algorithm was created to carry out Eqs. (5)–(13) computationally. To be more precise, the (ψ) angle was predicted by numerically solving Eq. (9) using the bisection method (Figure 9).

 

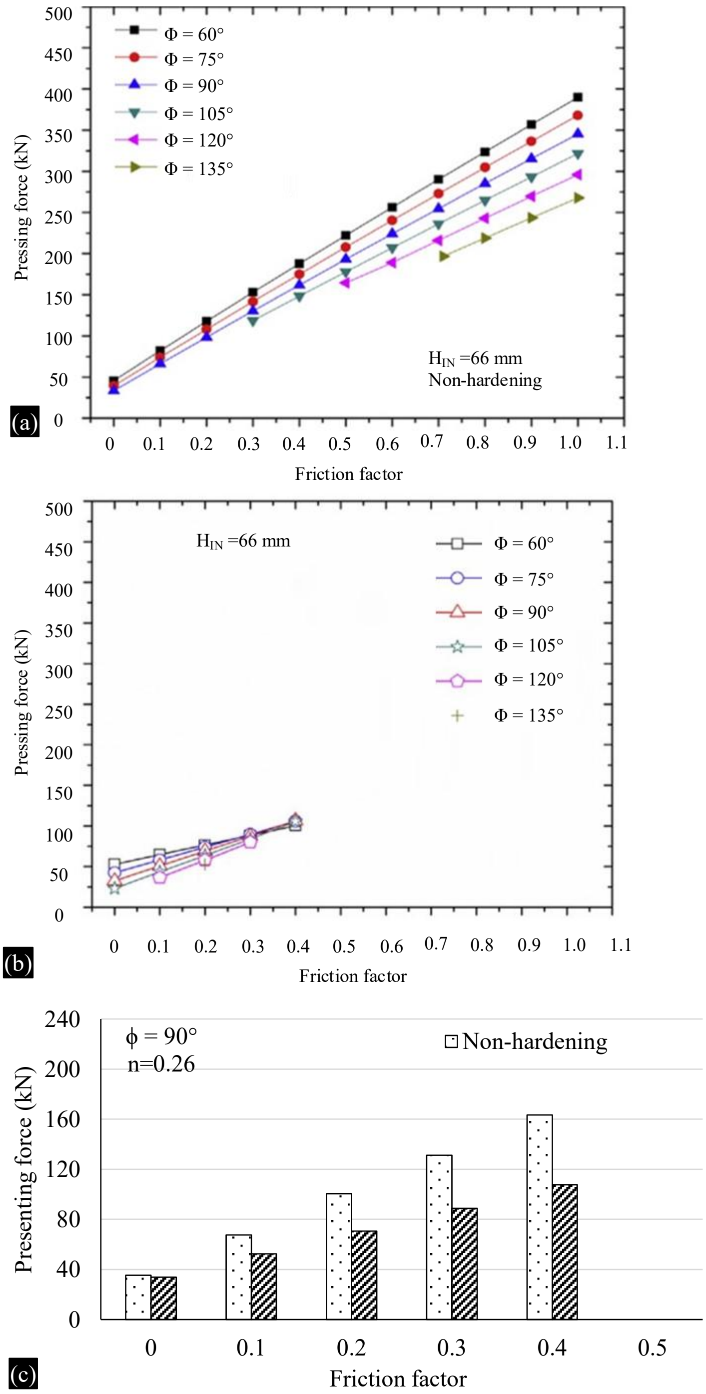


**Figure 8.** Alloys have analytical estimates of pressing force that take into consideration tribology and die channels angle (ϕ): (a) non-hardening AA5083, (b) hardening AA5083, and (c) a comparison between non-hardening and hardening alloys for (ϕ)=90° and m=0.18.

***Modelling with Plane-Strain Finite Elements***

In order to simulate the ECAP of an AA5083 billet at room temperature and predict the development of die corner angle, effective plastic strain, and pressing force during its forming, various friction conditions were taken into account. Finite element models for planar strain were created using the commercial software Ansys 14.0, taking into consideration the plastic behaviors of both non-hardening and work-hardening materials. The tooling was designed with the elastic qualities of H13 steel in mind, specifically a 200 GPa modulus of elasticity and a 0.3 Poisson's ratio. It was expected that the die was sharp and had no fillet radius, as shown in Figure 2. PLANE182 components were used to mesh the models. A total of 2033 fully integrated parts were used for the workpiece. The contact interfaces were characterized using the generalized Coulomb law and the augmented Lagrange approach. The von Mises criteria were utilized to estimate the maximum shear stress, which was derived from the uniaxial tension flow stress [17–20].

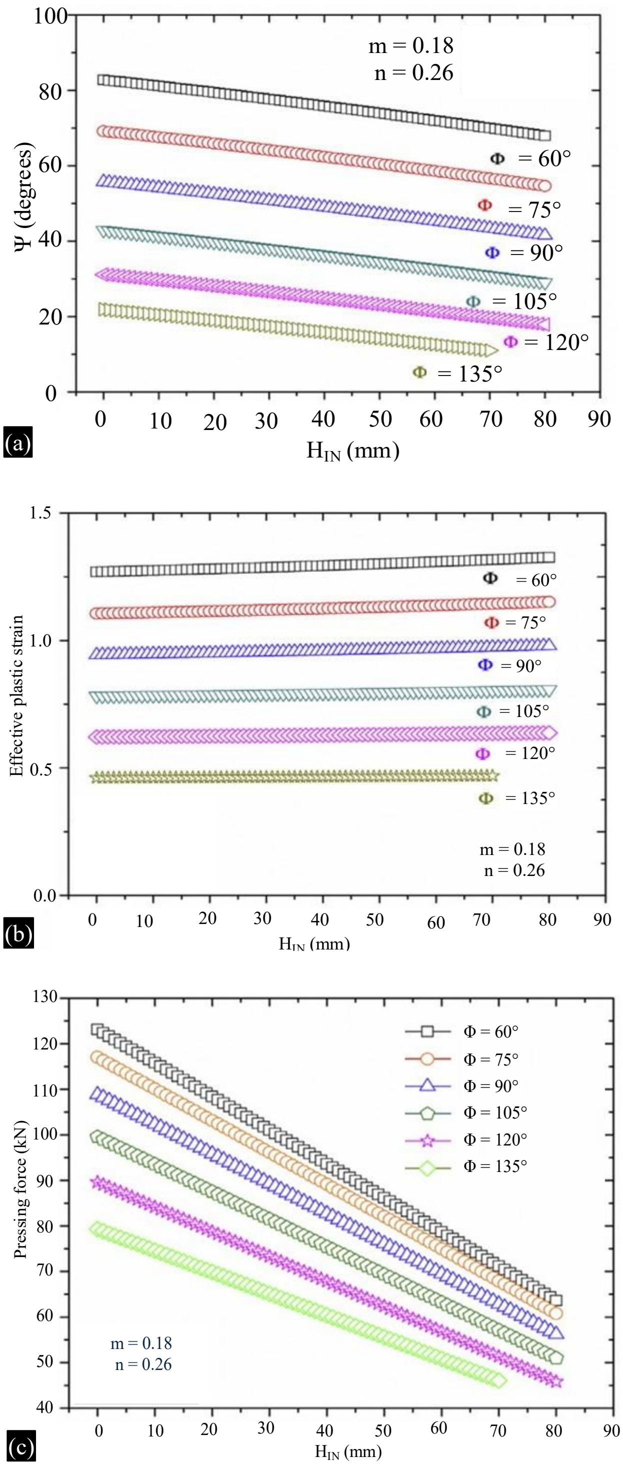


**Figure 9.** The following figures show how the analytically evaluated results varied depending on the die angle ($\phi$) and instantaneous billet height HIN for hardening AA5083: Pressing force, effective plastic strain, and angle ($\psi$) are the three variables.

 

Furthermore, it was determined using the von Mises criterion to be $\mu$=0.104 connected to a friction factor m=0.18⁄√3. As the materials moved into the horizontal die channel in increments of 0.10 mm up to 66 mm, both non-hardening and hardening materials were simulated. Vertical displacements along the workpiece's top line were set in order to accomplish this. The results of the pressing force were calculated with respect to the vertical response force, at intervals of 1 mm for billet displacement up to 66 mm.

## RESULTS AND DISCUSSION

The AA5083 material, which was tested under uniaxial tension, is related to the mechanical characteristics taken into account in this investigation. In the first instance, a die with zero die fillet radii and a fixed plunger velocity $V_0$ of 2.5 mm/s is used to evaluate the selected yield criteria and the effect of friction on the pressing pressure (*p*), initially presented for a die with $\phi$=90°. Next, by altering the dimensions of the billet and the geometry of the die, the correctness of the computations for Deformation time $t_D$ and effective plastic strain rate is validated. Assuming billet height and a frictionless condition of H=75 mm, the geometry of die configurations is defined by 60°⩽$\phi$⩽135°, 0≤$R_{inner}$≤$R_{outer}$=7.5 mm, 5≤L–W≤15 mm with a plunger velocity of 2.5 mm/s. By adjusting the die configuration, 60°⩽$\phi$⩽135°, 0⩽$R_{inner}$, $R_{outer}$⩽7.5 mm, investigations are conducted into how die geometry, friction conditions, and velocity affect pressing pressure (P). This entails maintaining the billet size at H=75 mm and L-W=15 mm while adjusting the friction factor 0⩽f⩽0.4 and plunger velocity 0.5⩽V_0⩽5 in mm/s. Additionally, the effective plastic strain is evaluated for 60°⩽$\phi$⩽135°, 0≤$R_{inner}$, $R_{outer}$≤7.5, using a plunger velocity and $V_0$=2.5 mm/s, H=75 mm, and L-W=15 mm for the billet dimensions. In summary, the predictions are influenced by the die geometry, frictional conditions, and process parameters of both (p) and ($\overline{\varepsilon^p}$) are categorized using the $2^k$ central composite factorial design in order of relevance. The billet dimensions of H=75 mm and L-W=15 mm are used for this. Table 1 lists all of the levels that have been assigned to each parameter [21, 22].

### Impact of The Strain-Rate Effects, Friction Factor, and Yield Criterion

The effects of the friction factor and the plasticity requirement, which are represented in terms of the ratio $k/\sigma_y$ and are set to 0.58 for von Mises isotropic descriptions and 0.54 for Drucker descriptions, on the ECAP pressure with ($\phi$=90°, $R_{inner}$=$R_{inner}$=0) mm and $V_0$=2.5 mm/s are shown in Figure 4. As expected, the frictional circumstances have a discernible direct effect; that is, the ECAP pressure rises significantly in proportion to the friction factor or, to a lesser degree, the yield stress ratio $k/\sigma_y$. The Drucker's yield surface flattens between the plane tension/compression states and the pure shear stress states, as seen in Figure 2. This flattening is responsible for the ratio $k/\sigma_y$ decline in comparison to the von Mises yield criterion. All analyses pertaining to pressing pressure predictions are then subjected to the Drucker isotropic yield criterion. Figure 5 illustrates how the size of the billet, the shape of the die, and the plunger velocity affect the effective plastic strain-rate and deformation time ($\tau_D$) under the assumption of a perfect frictionless state. First, as can be shown in Figure 5(a), the plastic strain-rate increases from 0.06 to 0.58 $s^{-1}$ as the billet dimensions are lowered or the punch velocity is increased. It can be shown from Figure 5(b) that there is an inverse relationship between $t_D$ and $V_0$. For a die composed of simply the outer radius, the same dependence has been seen, in agreement with finite element simulations. Figure 5(c and d) provides additional evidence for the connection between the behavior of the deformation time ($\tau_D$) and the impact of die geometry on the strain rate. Changes in die fillet radii have a greater impact on the strain rate than changes in the die intersection angle $\phi$. For 60°≤$\phi$≤135°, the strain rate increases from 0.012 to 0.013 $s^{-1}$ with variations in $R_{inner}/R_{outer}$=0, whereas for a very small change, it decreases from 0.012 to 0.096 $s^{-1}$ 0≤$R_{inner}/R_{outer}$≤1 With changes in 60°≤$\phi$≤135°, the strain rate goes from 0.012 to 0.013 $s^{-1}$; however, with a very slight change in $R_{inner}/R_{outer}$=0 it drops from 0.012 to 0.096 $s^{-1}$ and 0⩽$R_{inner}/R_{outer}$⩽1.

### Die geometry and ECAP Process Conditions' Effects

Figure 6 illustrates how the die configuration, friction, and punch velocity relate to the pressing pressure. Figure 6(a and b) demonstrates that the pressure rises from 304 to 476 MPa when the inner fillet radius increases in the direction of the outer one. When the angle ϕ increases from 60 to 135° for $R_{inner}/R_{outer}=1$, the pressure significantly decreases from 476 to 76 MPa. Likewise, when ϕ=60° is taken into account, the pressing pressure decreases from 682 to 476 MPa, and the outer fillet radius approaches the value. Consequently, the outer radius has a greater impact on the ECAP pressure and/or load. When the fillet radii are equal, the pressure also drops from 476 to 75 MPa with regard to the die intersection angle, suggesting that the ratios $R_{inner}/R_{outer}$ or $R_{outer}/R_{inner}$ have no bearing on the relationship between the channel angle (ϕ) and ECAP pressure. Lastly, the effects of the plunger velocity and the friction factor are displayed in Figure 6(c and d), respectively. As was already indicated, the pressure increases from 476 to 1390 MPa when the ϕ=60° value is increased from the frictionless to the sticking friction condition. In contrast to ϕ=60° and f=0, increasing the punch velocity from 0.5 to 5 mm/s results in a little increase in pressure. As shown in Figure 6(d), at a plunger velocity of $V_0=0$ mm/s, the pressing pressure rises from 456 to 1330 MPa, and the friction factor changes from 0 to 0.4. Thus, tribology, angle, fillet radii $V_0$, have an increasing degree of impact on the ECAP pressure estimates. Furthermore, there is a nonlinear influence on the pressure caused by variations in the die configuration, friction, and punch velocity. The way in which materials that are meant to harden under pressure behave. The relationship between the die geometrical configurations and the effective plastic strain is shown in Figure 7.

As it approaches the value for ϕ=60°, on the other hand, for $R_{inner}/R_{outer}=1.0$, the effective plastic strain rises from 1.6 to 2.0, as seen in Figure 7(a). The effective plastic strain predictions, however, decrease from 2.0 to 0.5. Figure 7(b) illustrates a decrease from 2.4 to 2.0 for ϕ=60° when Rinner is raised from 0 to $R_{inner}=7.5$ mm. In this case, $R_{inner}/R_{outer}=1.0$, as a function of the junction die channels angle, the plastic strain falls from 2.0 to 2.5 over the range of $60° \leqslant \phi \leqslant 135°$. The divergent behavior observed with changes in either $R_{inner}/R_{outer}=1.0$ is consistent with the expected behavior of the pressure, as shown in Figure 6(a and b). This alignment arises because the mean yield stress, as stated in Eq. (8), is significantly influenced by the effective plastic strain and, consequently, by modifications in the die's geometrical configurations (Figure 10).

**Variance Analysis and Surface Responses**

The study's of central composite design was linked to the variance ($F_0$) analysis. Under intense circumstances pressure (p), the influence of the parameters considered for the factorial design may be ranked using the order of significance. These variables are in the following order: plunger velocity ($V_0$), outer fillet radius $R_{outer}$, inner fillet radius $R_{inner}$, intersection die angle (ϕ), and friction factor m. Actually, as Figure 6 shows, the analysis of quadratic interactions between the parameters under consideration and pressing pressure demonstrates a nonlinear behavior with respect to die geometry and friction. The proposed surface response model's assumption of linearity explains why the fillet radii have less of an impact on the predictions of effective plastic strain than pressing pressure. The variance analysis, which accounts for the pure quadratic term, finds a linear relationship for effective plastic strain and nonlinear factor interactions for the pressing load (Figure 11) [23–27].

The comparison of $2^k$ results from the surface response modelling with the factorial predictions. It is clear from looking at the expected values that consideration must be given to the pure quadratic terms' nonlinear pressing pressure behavior (Figure 12). A second-order regression function is used to define the relevant surface response. On the other hand, the effective plastic stresses exhibit a linear dependence on the die geometrical parameters, in accordance with the first-order model. Figure 8 illustrates the connection between the pressing pressure and the intersection die angle of 90°, which is modelled using the axial and central factorial points. The pressure can be shown to decrease from 90 to 120 it moves from with the central, axial, and locations indicated by 69.5 and 140.35°. The quantitatively modelled pressing pressure estimates in relation to fillet radii variations are shown in Figure 9. Figure 9(a) illustrates the noteworthy finding of elevated pressing pressure associated with a rise in $R_{inner}$ as shown in Figure 9(b), the drop is noticeable with elevated values of $R_{outer}$. Figure 10 displays the modelled pressing pressure values in relation to changes in the friction factor and plunger velocity. According to Figure 10(a), which confirms the earlier finding in Figure 6(c), the pressure rises as the friction conditions worsen. However, a velocity increase (Figure 10(b)) contributes to the pressure rise from the center point on both the left and right sides, as can be seen in Figure 6(d). The linear and qualitative relationship between effective plastic strain and the ECAP die's geometry is shown in Figure 11. It is evident from Figure 11(a) that changes to the inner fillet radius $R_{inner}$ result in an increase in the effective plastic strain. Likewise, changes in the outer fillet radius $R_{outer}$ are accompanied by a commensurate drop in effective plastic strain, as seen in Figure 11(b).

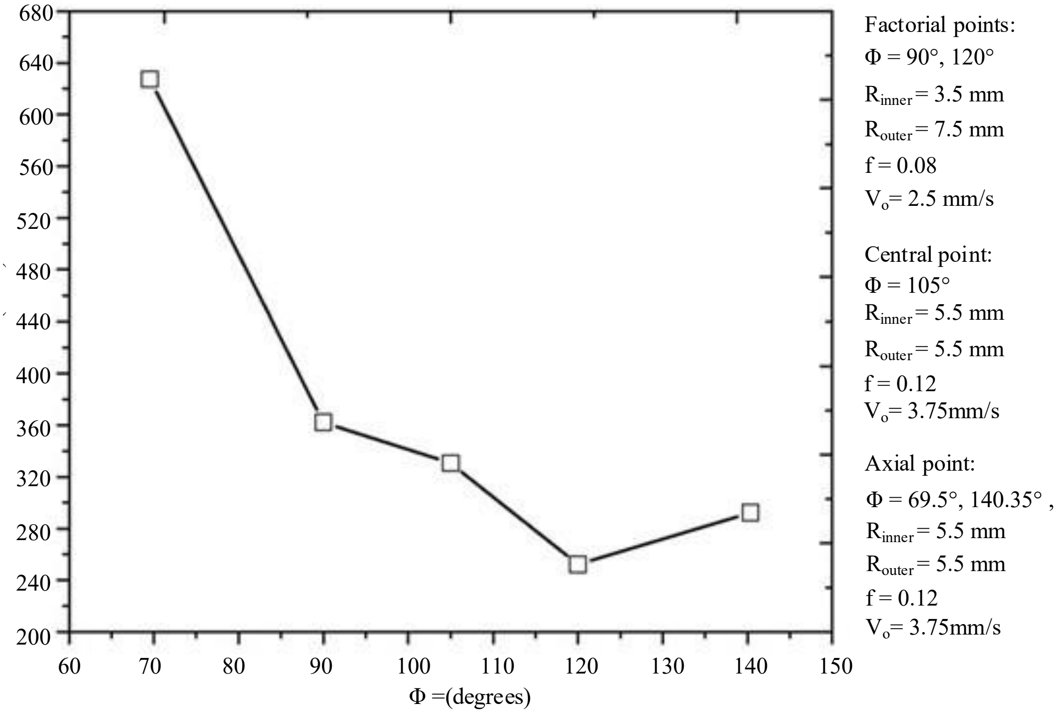


**Figure 10.** Factorial analysis $2^k$ was used to generate quantitative pressing pressure estimates as a function of the intersection angle of the die channels.

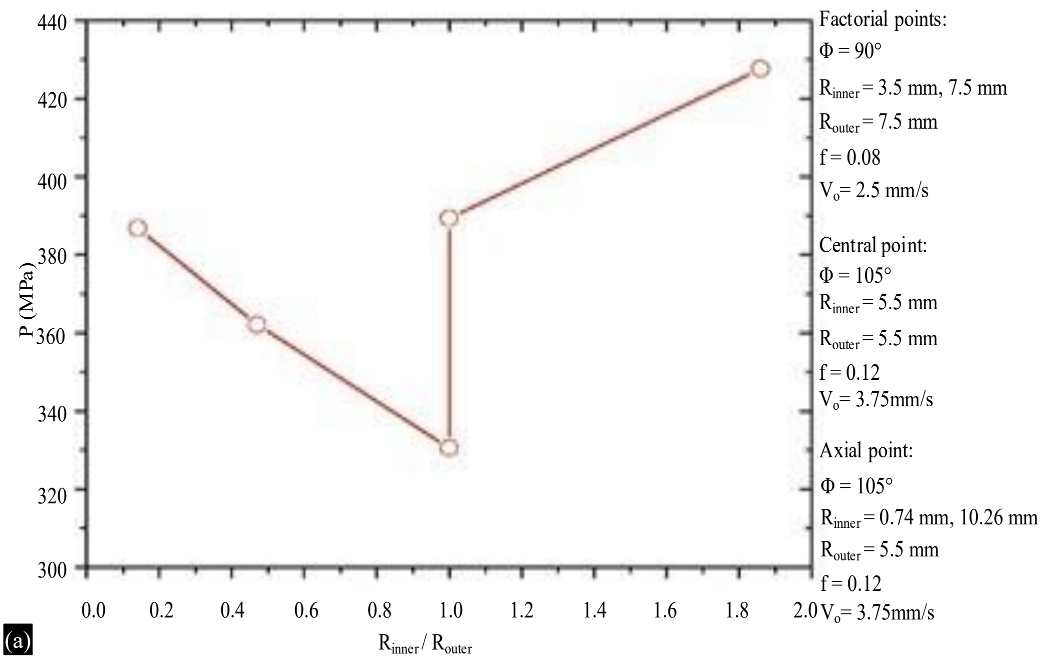

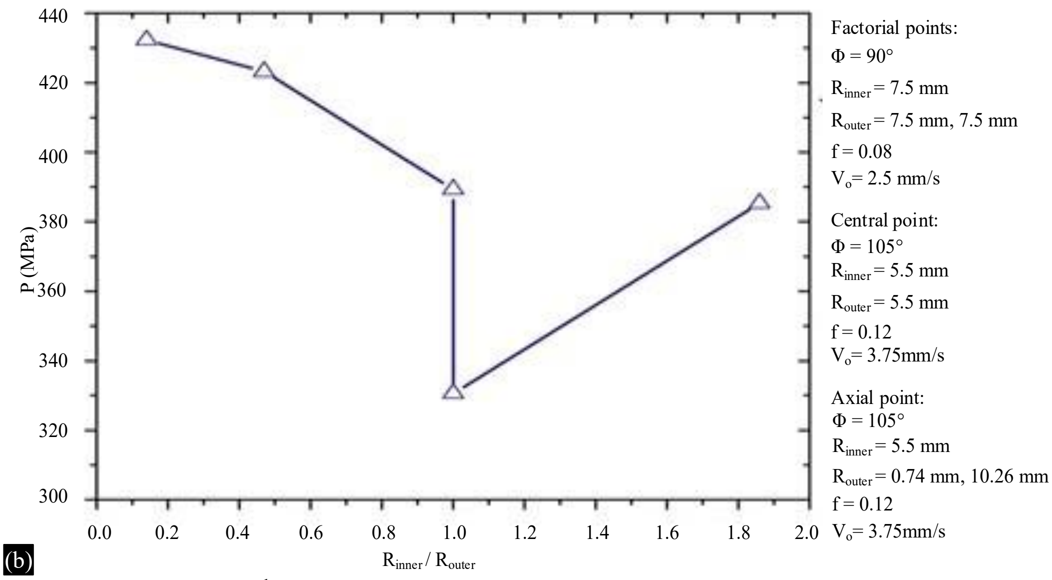


(b)

**Figure 11.** Factorial $2^k$ analysis yielded quantitative pressing pressure estimates as a function of (a) die inner fillet and (b) die outer fillet radii.

**Die Corner Gap Formation for Strain Hardening**

Figure 3 displays the analytical predictions of the die channel angles (ϕ) and angle (ψ) for different friction scenarios for both work-hardening and non-hardening AA5083. As shown in Figure 3(b), there was really a discernible rise in the value for a constant friction factor when taking into account a hardening exponent greater than zero for the alloy in question. This is because, in contrast to the non-hardening assumption shown in Figure 3(a), the material's mechanical strength diminishes.

Figure 4(a and b) illustrates this for each corresponding (ϕ) and m. Similarly, the difference between the results $\bar{\varepsilon}$ of non-hardening and hardenable AA5083 was less noticeable (1.15 and 1.03, respectively) because of trigonometric considerations. The pressing force predictions for AA5083's non-hardening and hardening behaviors are shown in Figure 5, which are based on changes in angle (ϕ) and friction levels. Generally speaking, the work-hardening condition decreased the needed load for material deformation when compared to the non-hardening condition, which is consistent with the different yield stresses that were taken into account in Eq. (6). Moreover, as shown in Figure 5(a and b), the effects of angle (ϕ) and tribology are similar to those previously mentioned for (ψ) and $\bar{\varepsilon}$. However, one important feature of Eq. (6) is that it may be applied to the critical friction factor of work-hardenable materials, as Figure 5(b) illustrates. This crucial friction factor was found to be 0.4 in the instance of AA5083. Within the range of 0 to 0.4, there was a decrease in pressing force $60° \leqslant \phi \leqslant 135°$. The literature has a wealth of documentation on this phenomenon. However, an increase in pressing force was noted within the range $135° \leqslant \phi \leqslant 60°$ of for m-values greater than 0.4. This happened when Eq. (6) contained the incompressibility factor used in the computation of $H_{OUT}$. When taking into account their combined influence together with the evaluation of the corresponding angle (ϕ), it was possible to identify the range of friction variables that produce consistent processing load outcomes. Additionally, with adjusted to 0.18, Figure 5(c) illustrates how material plastic behavior affects pressing force (ϕ)=90°. The processing load projections were larger in the absence of work-hardening than they were for hardenable AA5083.

The relationship between angle (ψ), pressing force, effective plastic strain, and the immediate height $H_{IN}$ of the billet for hardenable AA5083 is shown in Figure 6. This is seen when the friction factor is constant and the angle (ϕ) is varied. There was a steady drop in the angle (ψ) and a rise in the effective plastic strain.

 

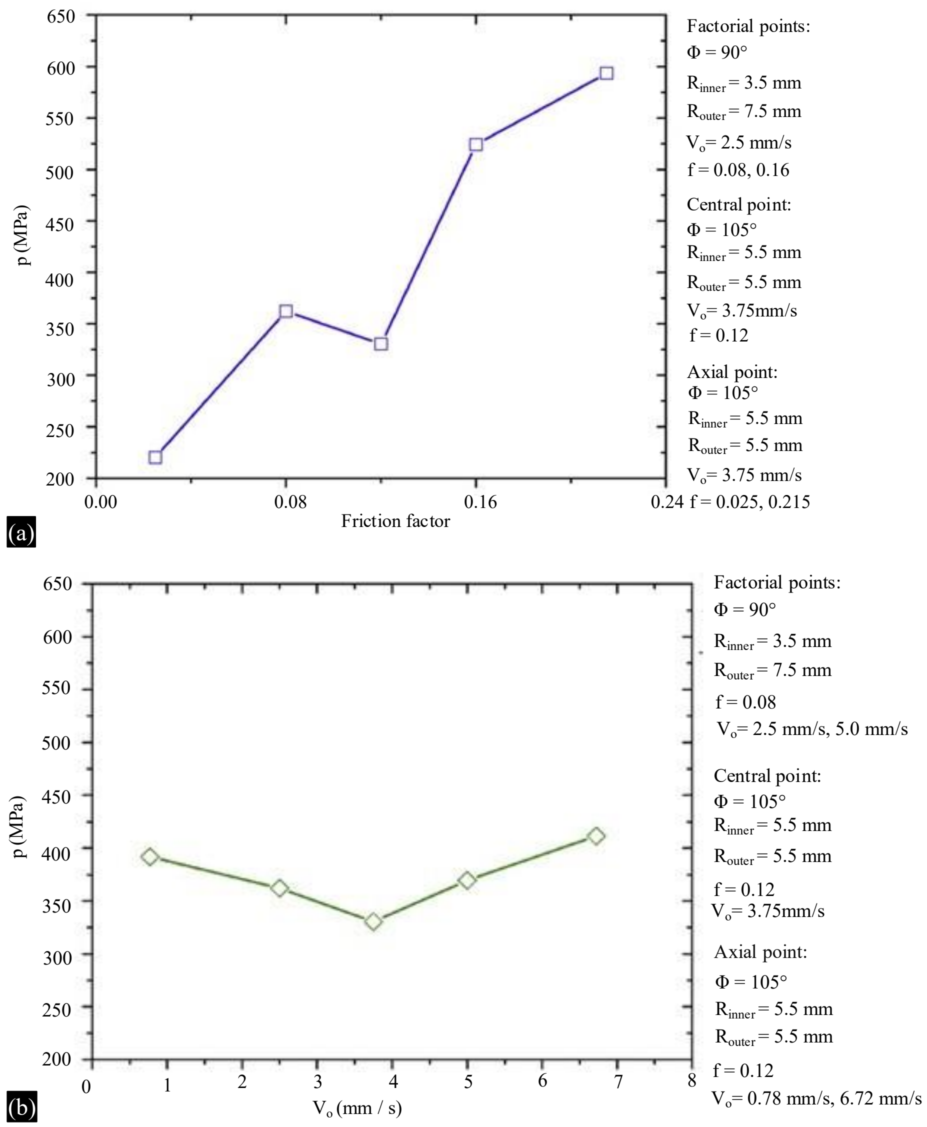


**Figure 12.** Factorial $2^k$ analysis yielded quantitative pressing pressure estimates as a function of (a) pressing velocity and (b) friction factor.

Additionally, higher initial values of $H_{IN}$ result in smaller pressing force values, aligning with the observations made by Pérez and Luri *et al*. [6]. This feature is illustrated in Figure 7. By contrasting the finite-element models with the experimental findings of Eivani and Karimi Taheri [13] for AA5083, the pressing force models were validated. In this comparison, m was set to 0.18, channels intersected at ($\phi$)=90°, and tooling was used without a fillet radius. The experimental force of 70 kN was selected for validation, and it was attained following a 15 mm billet movement. Thus, the proposed numerical models for both fully plastic AA5083 and work-hardened AA5083 yielded consistent and satisfactory outcomes, producing pressing force values of approximately 67 kN and 55 kN, respectively. It is evident that the work-hardenable plastic material with work-hardenable behavior needed less processing load after reaching its maximum force value than its non-hardened counterpart. There is also no doubt that the hardenable and non-hardenable curves produced by the numerical models show three separate phases (Figures 13–15).

First, the material is immediately squeezed within the first 5 mm of billet displacement; this is associated with the linear static friction domain. The second stage begins when the billet shifts, which occurs between 5 and 10 mm of displacement. The change from the static to the dynamic friction zones is represented by this phase. The third phase, which extends from 10 mm to the simulated end, represents the dynamic friction region. As a result, it is followed by a decrease in pressing force projections. The computed numerical results of angle (ψ) for the different material plastic behaviors are shown in Figure 8, and set to 0.18. As previously noted in the evaluation of the suggested analytical models, fully plastic materials cannot, because of their great mechanical resistance, produce appreciable curvatures at the intersection region of the die channels, as shown in Figure 3(a and b).

As such, the corresponding angles (ψ) are less than those found in materials that can be hardened, as these materials have a significant capacity for folding at the die deformation zone. Due to these factors, (ψ) the findings for the non-hardened AA5083 were approximately 5, whereas the work-hardened material had an estimated value of nearly 38. The average effective plastic strain predictions from Finite Elements and the corresponding standard deviation are shown in Figure 9. The die shape and friction conditions used in the pressing force calculations (Figure 7) and the angle estimation shown in Figure 8 were the same as those used in these predictions. It was expected that the deformation levels attributed to perfectly plastic materials would be bigger than those of hardenable AA5083, in accordance with the previously discussed issues about the angle (ψ). In the first case, a maximum average value of 1.25±0.3 was determined following 66 mm of billet displacement. The observed value for the second examined material's plastic behavior was 0.96±0.23 (Figure 16).

The validation of the suggested analytical models in terms of pressing power, angle (ψ), and effective plastic strain for both non-hardening and non-hardenable AA5083 is shown in Figure 10. By comparing the results with the matching Finite Element results (ϕ)=90° and holding constant at 0.18, this validation is accomplished.

In terms of material mechanical behavior, there is a general summary of the results that shows consistency between them. In particular, as compared to its work-hardened equivalent, AA5083 without hardening produces predictions for angle (ψ) that are smaller and figures for pressing force and effective plastic strain that are higher. Concurrently, the suggested theoretical models demonstrated satisfactory deviations from the corresponding numerical predictions, indicating a successful validation.

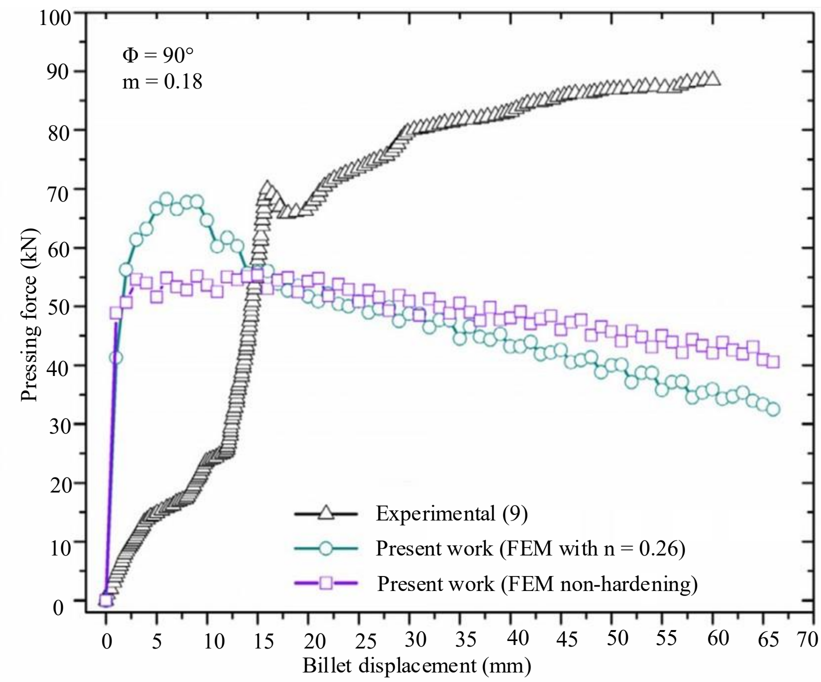


**Figure 13.** Finite-element pressing force predictions were compared to experimental findings obtained by Eivani and Karimi Taheri [13].

 

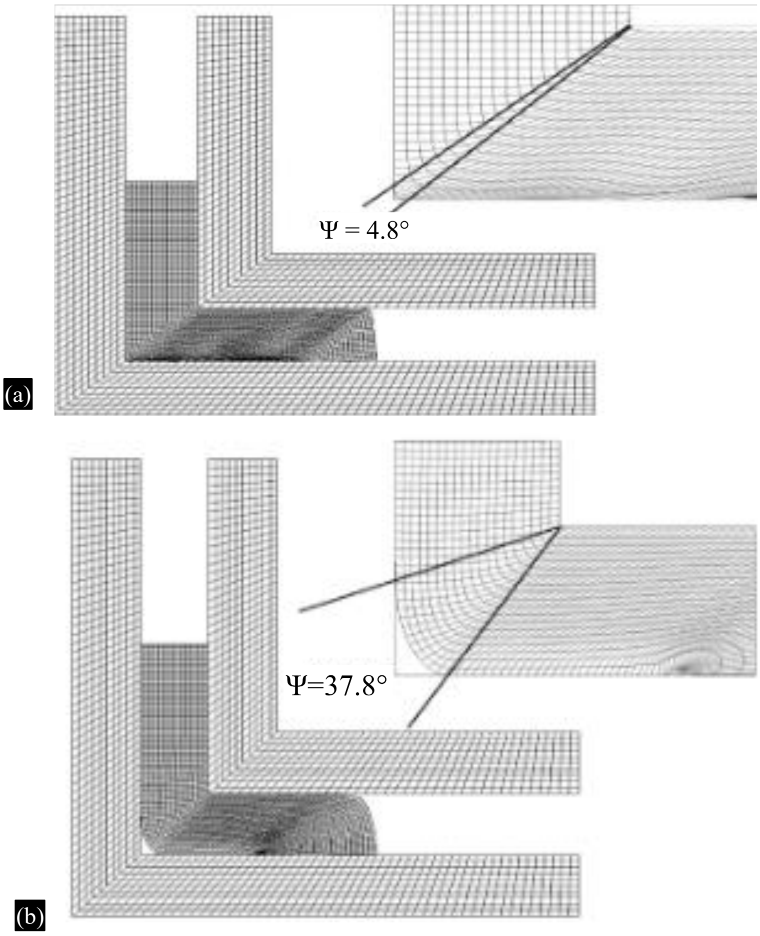


**Figure 14.** The study's numerical models, which are (a) non-hardening AA5083 and (b) hardening AA5083, produced the angle (ϕ) results.

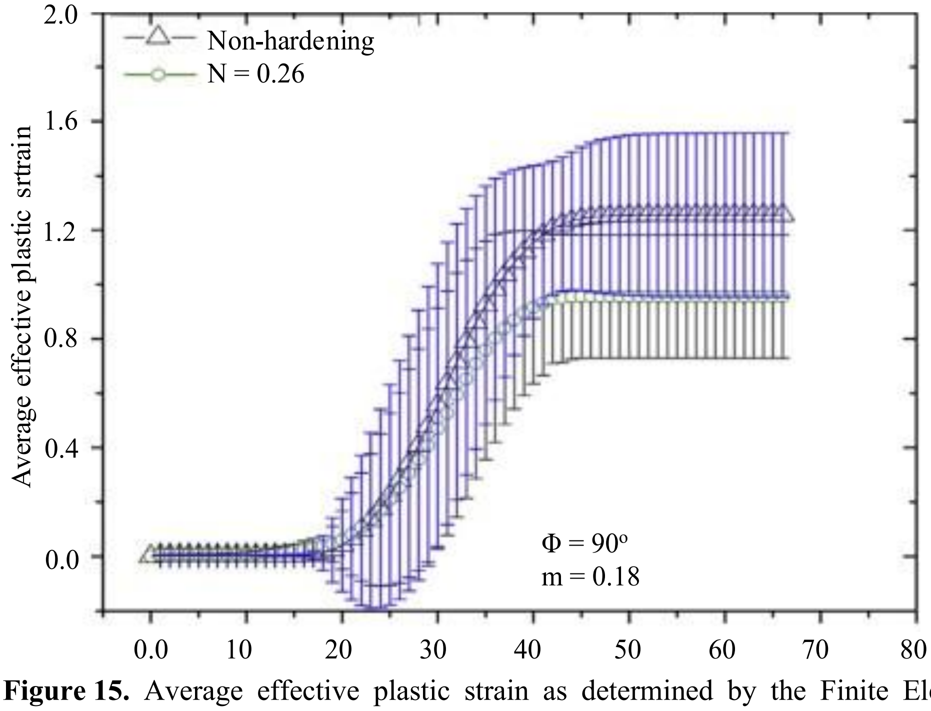


**Figure 15.** Average effective plastic strain as determined by the Finite Element Method (FEM): influence of material plastic behavior under constant friction conditions.

 

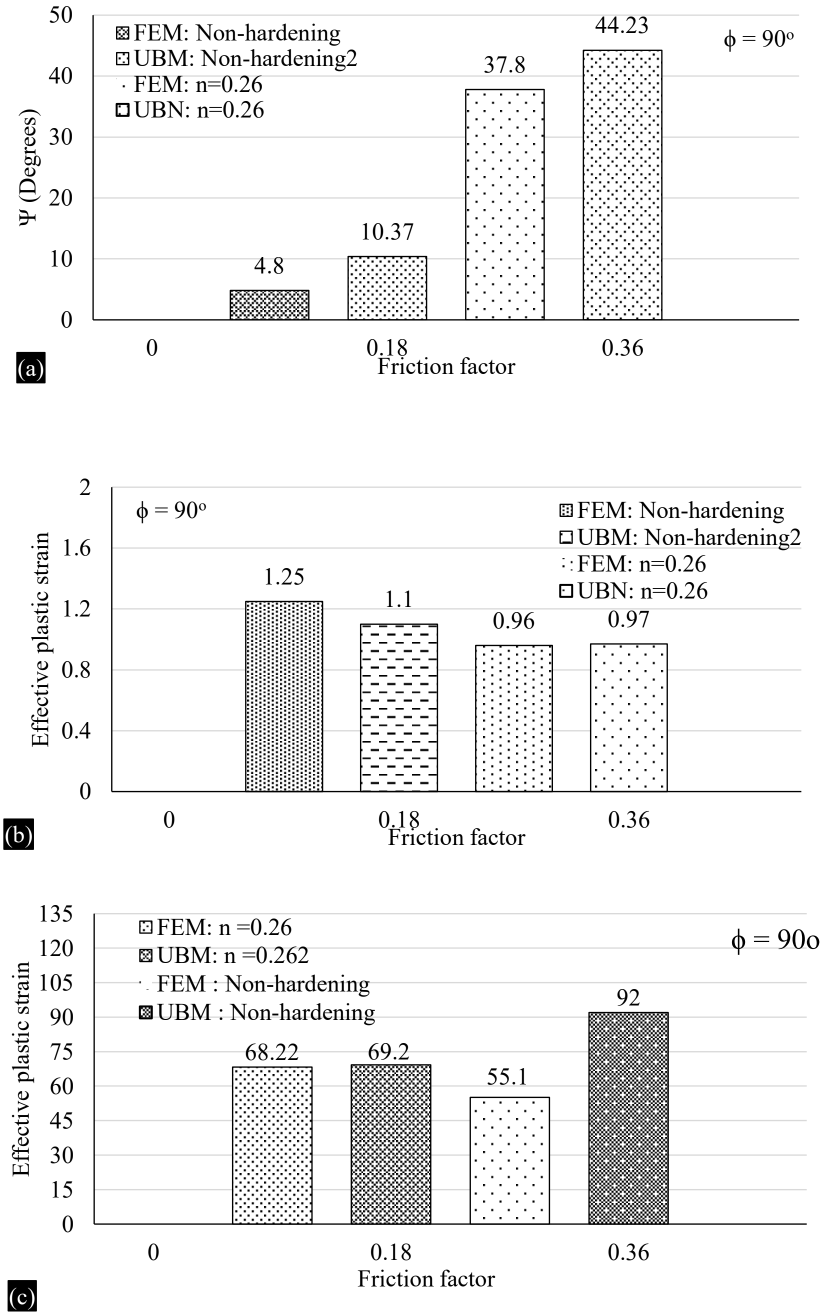


**Figure 16.** Validation of the analytical models (a) angle (ψ); (b) effective plastic strain; and (c) pressing force that are suggested for comparison with numerical data for hardening and non-hardening materials.

## CONCLUSION

Analytical analyses using the upper-bound method are presented in this work. These studies use two isotropic plasticity yield criteria and consider the effects of material strain rate to assess the pressing pressure and effective plastic strain. The analysis investigates the effects of die geometry, billet composition, and process variables on the predictions of pressing pressure and effective plastic strain during the processing of commercially pure aluminium. To further assess the significance of these parameters on the ECAP pressure and effective plastic strain, a central composite factorial design variance analysis was carried out. The relationship between pressing pressure and yield surface shape has helped to clarify the effects of friction conditions in the context of a single pass of ECAP at room temperature. The isotropic Drucker yield criterion is believed to be better suitable for reproducing pure shear and planar tension/compression stress states than the von Mises criterion. Therefore, its application in the analytical projections of FCC materials undergoing deformation utilizing ECAP is recommended. When material strain-rate sensitivity based on the total effective plastic strain and deformation time after a single pass of ECAP is included to the analytical solutions for pressing pressure, die geometry modifications, and the expected ECAP pressure agree. Considering modifications in plunger velocity, strain-rate effects on the reported pressing pressure behavior, and adjustments to the die geometry and friction conditions. The theoretical solutions developed in this study offer more precise load estimations for bulk material processing using the ECAP technique. The proposed composite factorial design makes it possible to classify significant variables that fundamentally influence the ECAP pressure or effective plastic strain. A nonlinear quantitative relationship between the parameters influencing pressing pressure was revealed by curvature research. Thus, a second-order function is believed to be more appropriate for modeling the pressing pressure surface response, but a multilinear regression model is recommended for the effective plastic strain. Based on the variance analysis and related surface reactions, the ECAP components that have a substantial impact on pressing pressure can be ranked in the following order of significance: In that order, the following factors are listed: (1) plunger velocity; (2) friction factor; (3) outer fillet radius; (4) inner fillet radius; and (5) intersection die channels angle. The theoretical results consistently demonstrated the effect of work hardening, which results in a rise in angle and a decrease in the expectations of effective plastic strain and pressing force. This comparison was carried out for AA5083 under the non-hardening assumption, accounting for various tooling shapes and friction conditions. Essential friction conditions could also be assessed for analytical pressing force data. It was also possible to investigate the impact of the immediate height of the billet entrance deformation zone on the responses for the strain-hardenable material while accounting for volumetric incompressibility. A comparison with published experimental results was used to validate the provided plane-strain finite element models with regard to processing load. They verified the increase in angle and decrease in effective plastic strain when contrasting work-hardened and non-hardened materials, attributing these changes to differences in mechanical behavior. By contrasting the observed consistency in analytical results for die corner angle, effective plastic strain, and pressing force with the corresponding predictions from finite element calculations, the proposed upper-bound solutions were validated.

## REFERENCES

1. Segal VM. Materials processing by simple shear. Mater Sci Eng: A. 1995; 197(2): 157–164. https://doi.org/10.1016/0921-5093(95)09705-8.
2. Iwahashi Yoshinori, et al. Principle of equal-channel angular pressing for the processing of ultra-fine grained materials. Scr Mater. 1996; 35(2): 143–146. https://doi.org/10.1016/1359-6462(96)00107-8.
3. Segal VM. Severe plastic deformation: simple shear versus pure shear. Mater Sci Eng: A. 2002; 338(1–2): 331–344. https://doi.org/10.1016/S0921-5093(02)00066-7.
4. Semiatin SL, Salem AA, Saran MJ. Models for severe plastic deformation by equal-channel angular extrusion. JOM. 2004; 56(10): 69–77. https://doi.org/10.1007/s11837-004-0296-y.
5. Segal VM. Equal channel angular extrusion: from macromechanics to structure formation. Mater Sci Eng: A. 1999; 271(1–2): 322–333. https://doi.org/10.1016/S0921-5093(99)00248-8.
6. Segal VM. Slip line solutions, deformation mode and loading history during equal channel angular extrusion. Mater Sci Eng: A. 2003; 345(1–2): 36–46. https://doi.org/10.1016/S0921-5093(02)00258-7.
7. Alkorta Jon, Javier Gil Sevillano. A comparison of FEM and upper-bound type analysis of equal-channel angular pressing (ECAP). J Mater Process Technol. 2003; 141(3): 313–318. https://doi.org/10.1016/S0924-0136(03)00282-6.
8. Luis Pérez CJ. On the correct selection of the channel die in ECAP processes. Scr Mater. 2004; 50(3): 387–393. https://doi.org/10.1016/j.scriptamat.2003.10.007.

9. Luis Pérez CJ. Upper bound analysis and FEM simulation of equal fillet radii angular pressing. Modelling Simul Mater Sci Eng. 2004; 12(2): 205. https://doi.org/10.1088/0965-0393/12/2/002.
10. Altan BS, Purcek G, Miskioglu I. An upper-bound analysis for equal-channel angular extrusion. J Mater Process Technol. 2005; 168(1): 137–146. https://doi.org/10.1016/j.jmatprotec.2004.11.010.
11. Stoica GM, et al. An analysis of the shear zone for metals deformed by equal-channel angular processing. Mater Sci Eng: A. 2005; 410–411: 239–242. https://doi.org/10.1016/j.msea.2005.08.186.
12. Luri R, et al. A new configuration for equal channel angular extrusion dies. J Manuf Sci Eng-Trans ASME. 2006; 128(4): 860–865. https://doi.org/10.1115/1.2194555.
13. Eivani AR, Karimi Taheri A. An upper bound solution of ECAE process with outer curved corner. J Mater Process Technol. 2007; 182(1–3): 555–563. https://doi.org/10.1016/j.jmatprotec.2006.09.021.
14. Eivani AR, Karimi Taheri A. The effect of dead metal zone formation on strain and extrusion force during equal channel angular extrusion. Comput Mater Sci. 2008; 42(1): 14–20. https://doi.org/10.1016/j.commatsci.2007.06.001.
15. Alkorta J, Sevillano JG. A comparison of FEM and upper-bound type analysis of equal-channel angular pressing (ECAP). J Mater Process Technol. 2003; 141(3): 313–318. https://doi.org/10.1016/S0924-0136(03)00282-6.
16. Barlat F. Crystallographic texture, anisotropic yield surface and forming limits of sheet metals. Mater Sci Eng. 1987; 91: 55–72. https://doi.org/10.1016/0025-5416(87)90283-7.
17. Eivani AR, Karimi Taheri A. An upper bound solution of ECAE process with outer curved corner. J Mater Process Technol. 2007; 182(1–3): 555–563.
18. Iwahashi Y, Wang W, Nemoto M, Langdon TG. Principle of equal-channel angular pressing for the processing of ultra-fine grained materials. Scr Mater. 1996; 35(2): 143–46.
19. Kobayashi S, Oh SI, Altan T. Metal Forming and the Finite-Element Method. New York: Oxford University Press; 1989.
20. Pérez CJL. Upper bound analysis and FEM simulation of equal fillet radii angular pressing. Modelling Simul Mater Sci Eng. 2004 a; 12(2): 205–214.
21. Pérez CJL. On the correct selection of the channel die in ECAP processes. Scr Mater. 2004 b; 50(3): 387–393.
22. Segal VM. Materials processing by simple shear. Mater Sci Eng A. 1995; 197(2): 157–64.
23. Srinivasan R. Computer simulation of the equichannel angular extrusion (ECAE) process. Scr Mater. 2001; 44(1): 91–96.
24. Valiev RZ, Islamgaliev RK, Alexandrov IV. Bulk nanostructured materials from severe plastic deformation. Prog Mater Sci. 2000; 45(2): 103–89.
25. Valiev RZ, Langdon TG. Principles of equal-channel angular pressing as a processing tool for grain refinement. Prog Mater Sci. 2006; 51(7): 881–981.
26. Zhao G, Xu S, Luan Y, Guan Lun N, Ren X. Grain refinement mechanism analysis and experimental investigation of equal channel angular pressing for producing pure aluminum ultra-fine grained materials. Mater Sci Eng A. 2006; 437(2): 281–292.
27. Zhang ZJ, Son IH, Im YT, Park JK. Finite element analysis of plastic deformation of CP-Ti by multipasss equal channel angular extrusion at medium hot-working temperature. Mater Sci Eng A. 2007; 447(1–2): 134–141.

 